Derbylite and graeserite from the Monte Arsiccio mine (Apuan Alps, Tuscany, Italy): occurrence and crystal-chemistry

CRISTIAN BIAGIONI[1*], ELENA BONACCORSI[1], NATALE PERCHIAZZI[1], ULF HÅLENIUS[2], and FEDERICA ZACCARINI[3]

[1]*Dipartimento di Scienze della Terra, Università di Pisa, Via Santa Maria 53, 56126 Pisa, Italy*
[2]*Department of Geosciences, Swedish Museum of Natural History, Box 50007, SE-10405 Stockholm, Sweden*
[3]*Department of Applied Geological Sciences and Geophysics, University of Leoben, Peter Tunner Str. 5, A-8700 Leoben, Austria*

**e-mail address*: cristian.biagioni@unipi.it

Mineralogical Society

This is a 'preproof' accepted article for Mineralogical Magazine. This version may be subject to change during the production process.
DOI: 10.1180/mgm.2020.67

ABSTRACT

New occurrences of derbylite, $Fe^{2+}_{x}Fe^{3+}_{4-2x}Ti^{4+}_{3+x}Sb^{3+}O_{13}(OH)$, and graeserite, $Fe^{2+}_{x}Fe^{3+}_{4-2x}Ti^{4+}_{3+x}As^{3+}O_{13}(OH)$, have been identified in the Monte Arsiccio mine, Apuan Alps (Tuscany, Italy). Derbylite occurs as prismatic to acicular black crystals in carbonate veins. Iron and Ti are replaced by V (up to 0.29 atoms per formula unit, apfu) and minor Cr (up to 0.04 apfu). Mössbauer spectroscopy confirmed the occurrence of Fe^{2+} (up to 0.73 apfu), along with Fe^{3+}. The Sb/(As+Sb) atomic ratio range between 0.73 and 0.82. Minor Ba and Pb (up to 0.04 apfu) occur. Derbylite is monoclinic, space group $P2_1/m$, with unit-cell parameters a 7.1690(3), b 14.3515(7), c 4.9867(2) Å, β 104.820(3)°, V 495.99(4) Å^3. The crystal structure was refined to R_1 = 0.0352 for 1955 reflections with $F_o > 4\sigma(F_o)$. Graeserite occurs as prismatic to tabular black crystals, usually twinned, in carbonate veins or as as porphyroblasts in schist. Graeserite in the first kind of assemblage is V-rich (up to 0.66 apfu), whereas it is V-poor in the second one (0.03 apfu). Along with minor Cr (up to 0.06 apfu), this element replaces Fe and Ti. The occurrence of Fe^{2+} (up to 0.68 apfu) is confirmed by Mössbauer spectroscopy. Arsenic is dominant over Sb and detectable amounts of Ba and Pb have been measured (up to 0.27 apfu). Graeserite is monoclinic, space group $C2/m$. Unit-cell parameters are a 5.0225(7), b 14.3114(18), c 7.1743(9) Å, β 104.878(3)°, V 498.39(11) Å^3 and a 5.0275(4), b 14.2668(11), c 7.1663(5) Å, β 105.123(4)°, V 496.21(7) Å^3. The crystal structures of two graeserite samples were refined to R_1 = 0.0399 and 0.0237 for 428 and 1081 reflections with $F_o > 4\sigma(F_o)$, respectively. Derbylite and graeserite have homeotypic relations. They share the same tunnel structure, characterized by an octahedral framework and cuboctahedral cavities, hosting $(As/Sb)O_3$ groups and (Ba/Pb) atoms.

Keywords: derbylite, graeserite, antimonite, arsenite, iron, titanium, crystal structure, Monte Arsiccio, Apuan Alps, Italy.

Introduction

Since the middle of the 19th Century, the hydrothermal veins hosted within the metamorphic rocks belonging to the Apuan Alps Metamorphic Complex (northern Apennines, Italy) have been known for the occurrence of many thioantimonite and thioarsenite mineral species (the so-called "sulfosalts", with trivalent Sb or As, respectively – Moëlo *et al*., 2008). On the contrary, the only antimonite species known to date is derbylite, reported from the Buca della Vena mine since the beginning of the 1980s (Mellini *et al*., 1983). Derbylite, ideally $Fe^{3+}_4Ti^{4+}_3Sb^{3+}O_{13}(OH)$, was first found by Hussak and Prior (1895) in the cinnabar-bearing gravels of the fazenda Três Cruzes, Tripuí (formerly Tripuhy), Ouro Preto (Minas Gerais, Brazil) and described by the same authors as a new mineral species two years later (Hussak and Prior, 1897). Its crystal structure was solved by Moore and Araki (1976) in the space group $P2_1/m$ down to $R_1 = 0.045$. Mellini *et al*. (1983) provided modern chemical data, suggesting the occurrence of the substitution mechanism $2Fe^{3+} = Fe^{2+} + Ti^{4+}$, and revising the chemical formula of derbylite to $Fe^{2+}_xFe^{3+}_{4-2x}Ti^{4+}_{3+x}Sb^{3+}O_{13}(OH)$. Later, Mellini *et al*. (1986) discussed the occurrence of V^{3+} replacing Fe^{3+} in other samples from the Buca della Vena mine.

The mineralogical studies carried out since the end of the 2000s on the mineral assemblages from the Monte Arsiccio mine, a locality placed just a few km south-west with respect to Buca della Vena, in a similar geological setting, allowed an additional identification of derbylite from the Apuan Alps and a new finding of its arsenite analogue, graeserite, ideally $Fe^{3+}_4Ti^{4+}_3As^{3+}O_{13}(OH)$. This latter mineral was first described by Krzemnicki and Reusser (1998) from the Binn Valley, Switzerland, and its crystal structure was solved by Berlepsch and Armbruster (1998). Graeserite is homeotypic with derbylite, showing a different space group symmetry, i.e., $C2/m$ (assuming the standard setting).

The finding of derbylite and graeserite at the Monte Arsiccio mine allowed to refine the knowledge of the crystal-chemistry of these unusual Sb and As oxysalts, merging the chemical and structural data with Mössbauer spectroscopic information. In this paper, the results of this study are reported.

Experimental

Studied samples

Specimens of derbylite and graeserite were collected at the Sant'Olga and Sant'Anna levels of the Monte Arsiccio mine. In the former, derbylite (samples A-D) and graeserite (samples E-F) occur in veins hosted within pyrite- and magnetite-rich metadolostone, along with other rare minerals; in the latter, only graeserite was found (sample G), as porphyroblasts within schist. The studied samples (Fig. 1) are representative of some different mineral assemblages or morphologies shown by derbylite and graeserite from this locality. A description of the studied samples and the mineral association is given in Table 1. Sample A contains another antimonite, stibivanite, ideally $V^{4+}Sb^{3+}_2O_5$, which occurs also in sample F where it is associated with the new diarsenite mineral bianchiniite, ideally $Ba_2(TiV)(As_2O_5)_2OF$ (Biagioni *et al*., 2019).

Chemical data

Quantitative chemical data were collected on derbylite and graeserite samples using a Superprobe JEOL JXA 8200 electron microprobe at the "Eugen F. Stumpfl" laboratory (Leoben University, Austria). The following analytical conditions were used: WDS mode, accelerating voltage 20 kV, beam current 10 nA, beam size 1 μm. The following standards (element, emission line) were used: rutile (Ti *K*α), synthetic vanadium (V *K*α), chromite (Cr *K*α), magnetite (Fe *K*α), skutterudite (As *L*α), stibnite (Sb *L*α), baryte (Ba *L*α), and galena (Pb *M*α). The following diffracting crystals were selected: LIFH for Ti, V, Cr, and Fe; TAP for As; PETJ for Ba, and PETH for Sb and Pb. Fluorine was sought but found below the detection limit. The ZAF routine was applied for the correction of the raw data. Counting times were 20 s for peak and 10 s for left and right backgrounds. Chemical data are given in Table 2.

Mössbauer spectroscopy

The ^{57}Fe Mössbauer spectra of two selected derbylite and graeserite samples (samples C and F, respectively, for which sufficient homogeneous material was available) were collected at room temperature in transmission mode using a ^{57}Co (in Rh matrix) point source, with a nominal activity of 0.40 GBq (Swedish Museum of Natural History, Stockholm, Sweden). Absorbers were prepared by gently grinding sample material (in the range 0.1-0.2 mg), which was placed in a ~2×2 mm square on a strip of tape and positioned closely in front of the point source. The Mössbauer spectra were acquired over the velocity range ± 4 mm/s and were calibrated against α-Fe foil. The spectra, shown in Figure 2, were fitted using the program MossA (Prescher *et al*., 2012). Hyperfine parameters are given in Table 3.

Crystallography

Single-crystal X-ray diffraction data were collected on derbylite (sample C) and graeserite (samples F and G) using a Bruker Smart Breeze diffractometer equipped with an air-cooled Photon II CCD detector, with graphite-monochromatized Mo *K*α radiation. The detector-to-crystal distance was set at 50 mm. Data were corrected for Lorentz-polarization factors and absorption using the package of softwares *Apex*3 (Bruker AXS Inc., 2016).

Derbylite is monoclinic, space group $P2_1/m$, with unit-cell parameters a = 7.1690(3), b = 14.3515(7), c = 4.9867(2) Å, β = 104.820(3)°, V = 495.99(4) Å^3. These values can be compared with those reported by Moore and Araki (1976), i.e., a = 7.160(1), b = 14.347(3), c = 4.970(1) Å, β = 104.61(2)°, V = 494.0(2) Å^3, and Mellini *et al*. (1983), i.e., a = 7.156(2), b = 14.354(4), c = 4.980(1) Å, β = 104.69(2)°, V = 494.8(2) Å^3.

Unit-cell parameters of the two samples of graeserite are a = 5.0225(7), b = 14.3114(18), c = 7.1743(9) Å, β = 104.878(3)°, V = 498.39(11) Å^3 (sample F) and a = 5.0275(4), b = 14.2668(11), c = 7.1663(5) Å, β = 105.123(4)°, V = 496.21(7) Å^3 (sample G). These values can be compared with those reported by Berlepsch and Armbruster (1998): a = 5.0053(4), b = 14.272(1), c = 7.1736(6) Å, β = 105.165(2)°, V = 494.61(7) Å^3. The examination of systematic absences confirmed the space group $C2/m$ for graeserite samples.

The crystal structures of derbylite and graeserite were refined using *Shelxl*-2018 (Sheldrick, 2015) starting from the atomic coordinates given by Moore and Araki (1976) and Berlepsch and Armbruster (1998) for derbylite and graeserite, respectively. Scattering curves

for neutral atoms were taken from the *International Tables for Crystallography* (Wilson, 1992).

The first step of refinement of derbylite converged to R_1 = 17.8%, showing a high electron density residual corresponding to another position of Sb. After its addition, the R_1 dropped to 8.4%. The site scattering of the two Sb positions have been refined using the Sb *vs* As scattering curves at the Sb(a) and Sb(b) sites, respectively, in order to take into account the occurrence of both Sb and As, as indicated by electron microprobe data, and constraining the sum of Sb and As to be 1 apfu. The site scattering at the four independent octahedral *M*(1)–*M*(4) sites was refined using the Ti *vs* Fe scattering curves. Actually, Moore and Araki (1976) refined the *M*(1) site as a pure Ti position. On the contrary, the relatively low U_{eq} value suggested the occurrence of a heavier atom replacing Ti. In this way, the refinement was improved to R_1 = 5.6%, lowered to 5.1% assuming an anisotropic model for both cations and anions. At this stage of refinement, a relatively high maximum close to (0, ¼, ¼) was observed. Adding this residual, interpreted as a partially occupied Ba position, the refinement converged to R_1 = 3.52% for 1955 reflections with $F_o > 4\sigma(F_o)$ and 116 refined parameters.

The refinement of sample F of graeserite rapidly converged to R_1 = 8.6%, confirming the correctness of the structural model. The site scattering of the three independent *M* sites was freely refined using the scattering curves of Ti *vs* Fe. Whereas *M*(1) was found fully occupied by Ti only, the *M*(2) and *M*(3) sites have a mixed (Ti,Fe) occupancy. The scattering curves of As *vs* Sb were used for the As site, whereas the site occupancy at the Ba site was freely refined. The anisotropic model (with the only exception being represented by the Ba site that was refined isotropically) converged to R_1 is 4.04%. In the last stage of the refinement, the occurrence of an electron density residual close to the As site suggested a possible splitting of this position between As- and Sb-centered sites. The refinement finally converged to R_1 = 3.99% for 428 reflections with $F_o > 4\sigma(F_o)$ and 68 refined parameters.

During the first step of the refinement of the crystal structure of sample G, the additional Ba position was removed. The refinement converged to a high R_1 value of 24.8%, showing a high maximum at coordinates (-½,½, 0). Adding this maximum [labeled Ba(1)], the refinement converged to R_1 = 8.2%, with the occurrence of another significant residual close to Ba(1). The addition of this further maximum [initially labeled Ba(2)] lowered the R_1 value to 5.2%. The same site scattering curves used for sample F were used. All three *M* sites revealed a mixed (Ti,Fe) occupancy. The structural model was refined anisotropically (except for the Ba sites) down to R_1 = 2.50%. Finally, the site occupancy of Ba(2) was modelled using the scattering curve of Pb *vs* □, taking into account the asymmetric coordination of this atom, likely related to the lone-electron-pair activity of Pb^{2+}; for this reason the site was relabeled as Pb(2). This improved the R_1 to a final value of 2.37% for 1081 reflections with $F_o > 4\sigma(F_o)$ and 69 refined parameters.

Details of the intensity data collections and crystal structure refinements are given in Table 4.

Results and discussion

Chemical formula of derbylite and graeserite

Moore and Araki (1976) proposed the normalization of the chemical formula of derbylite based on 27 negative charges (i.e., 13 O^{2-} and one OH^-) and eight cations. However,

the occurrence of other elements like Ba and Pb poses some questions about the actual normalization factor. Grey *et al*. (1987) and Berlepsch and Armbruster (1998) showed that Ba and Pb occur in cuboctahedral cavities, in agreement with their larger ionic radii in six-fold coordination (1.35 and 1.19 Å, respectively – Shannon, 1976) compared with those of Fe^{2+} and Ti^{4+} (0.78 and 0.605 Å, respectively – Shannon, 1976).

Tomichite, $(V,Fe)^{3+}{}_4Ti^{4+}{}_3As^{3+}O_{13}(OH)$, is an arsenite close to graeserite, which can contain minor Ba (Nickel and Grey, 1979; Grey *et al*., 1987). According to Grey *et al*. (1987) the increasing Ba content in Ba-rich tomichite is coupled with the replacement of Ti^{4+} by $(V,Fe)^{3+}$, likely according to the substitution $2Ti^{4+} + \square = 2(V,Fe)^{3+} + Ba^{2+}$. Grey *et al*. (1987) adjusted the Fe^{2+}/Fe^{3+} ratio in order to achieve the electrostatic balance, without any direct measurement of this ratio. Their chemical data apparently fit with this substitution mechanism, showing quite different Fe^{2+}/Fe^{3+} ratios among the three studied samples. On this basis, they proposed the end-member composition $Ba_{0.5}(As_2)_{0.5}Ti_2(V,Fe)_5O_{13}(OH)$ for barian tomichite. Figure 3a shows the relationships between Ti^{4+} and (Ba+Pb) atoms per formula unit (apfu) in the samples from Monte Arsiccio. The (Ba,Pb)-poorest samples (derbylite samples) are relatively enriched in Ti^{4+}, whereas the (Ba,Pb)-enriched compositions (graeserite samples) are slightly depleted in Ti^{4+}. However, there is not a clear linear relationship between (Ba+Pb) and Ti apfu. According to Mellini *et al*. (1983), the Ti content is also coupled with the Fe^{2+} content.

Table 2 gives the results of Mössbauer spectroscopy performed on two selected samples of derbylite (sample C) and graeserite (sample F) from Monte Arsiccio. No significant differences between the two samples were observed as regards the Fe^{2+}/Fe^{3+} atomic ratios, i.e., 0.19/0.81 in derbylite and 0.21/0.79 in graeserite. Within experimental uncertainties, the two samples have the same Fe^{2+}/Fe^{3+} atomic ratio. Notwithstanding different Ba contents, the total amount of Ti is very similar (3.67 and 3.68 apfu for samples C and F, respectively), as well as the sum of trivalent metals (2.63 and 2.65 apfu for samples C and F, respectively). This seems to disagree with the hypothesis of Grey *et al*. (1987). Moreover, the negative relation between ∑(Fe,V,Cr) *vs* Ti occur in both derbylite and graeserite, as shown in Figure 3b.

Barium and Pb are positively correlated with the As^{3+} content (Fig. 3c). This may be surprising, since Ba and As occupy the same cuboctahedral cavities. However, as discussed by Grey *et al*. (1987) and Berlepsch and Armbruster (1998), the occurrence of Ba and Pb within these cavities seems to be coupled with the occurrence of two AsO_3 groups within other cavities. Indeed, whereas derbylite has a very low Ba and Pb content, owing to the larger size of Sb, that does not allow the accommodation of two SbO_3 groups within a cuboctahedral cavity, As-minerals related to derbylite (e.g., graeserite, tomichite) show larger contents of divalent large-radius cations like Ba and Pb and the sum of (As+Sb) with (Ba+Pb) exceeds one apfu.

Arsenic and Sb are negatively correlated (Fig. 3d). Minor vacancies at the (As/Sb) sites have been observed both in derbylite and graeserite. Usually, they are up to 0.06 apfu. If they are real (and not the result of experimental uncertainties), they could be balanced through the substitution $(As/Sb)^{3+} + 3O^{2-} = \square + 3OH^-$.

On the basis of these considerations, the chemical formulae of derbylite and graeserite have been recalculated on the basis of $(Fe^{2+} + Fe^{3+} + V^{3+} + Cr + Ti) = 7$ apfu, distributing Fe^{2+}

and Fe^{3+} on the basis of 24 positive charges and assuming the trivalent oxidation state for V. Hydroxyl groups were calculated on the basis of electrostatic neutrality, assuming the substitution mechanism $(As/Sb)^{3+} + O^{2-} = (Ba/Pb)^{2+} + OH^-$ and $(As/Sb)^{3+} + 3O^{2-} = \square + 3OH^-$. The results are given in Table 2 and crystal-chemical formulae are reported in the foot-note of the same Table.

It is interesting to compare the results of such a calculation procedure with the Fe^{2+}/Fe_{tot} atomic ratios measured through Mössbauer spectroscopy (Table 3). The sample of derbylite (sample C) has a Fe^{2+}/Fe_{tot} atomic ratio of 0.19(2), to be compared with 0.22 obtained through the recalculation procedure. In graeserite (sample F), an atomic ratio of 0.21(2) was measured, to be compared with a calculated value of 0.25. The two values are within the experimental uncertainties.

Crystal structure of derbylite and graeserite

In agreement with previous authors (e.g., Berlepsch and Armbruster, 1998), the crystal structure of derbylite and graeserite can be described as a tunnel structure, with the tunnel walls formed by α-PbO_2-type double octahedral chains and the top and the bottom by V_3O_5-type octahedral columns (Fig. 4). Due to the different width of the V_3O_5-type columns, which varies between one and two octahedra, the tunnel width expands and contracts along its direction. In this way, cuboctahedral cavities can be identified, occupied by (As/Sb) or (Ba/Pb).

Derbylite

Atomic coordinates, site occupancies, and equivalent isotropic displacement parameters of derbylite are given in Table 5, whereas selected bond distances are reported in Table 6. A comparison between refined and calculated site scatterings at the cation sites, along with proposed site populations and observed and calculated average distances are given in Table 7. Table 8 reports the bond-valence sums (BVS), calculated using the site populations given in Table 7 and the bond parameters of Brese and O'Keeffe (1991) for all the pair cation–anion, the only exception being Sb^{3+}, for which the bond parameters of Mills *et al*. (2009) were used.

The octahedral framework is formed by four independent *M*(1)–*M*(4) sites, whereas three partially filled sites occur in the cuboctahedral cavities. The *M*(1) octahedron is quite regular, with average bond distance of 1.992 Å (range 1.973 – 1.999 Å), to be compared with 1.962 Å reported by Moore and Araki (1976). In addition, the difference between the longest and shortest distance, Δ*d*, is 0.026 Å and 0.061 Å for the samples from Monte Arsiccio and that studied by Moore and Araki (1976), respectively. It is well-known that Ti^{4+}-centered octahedron are usually distorted, owing to the off-center displacement of this cation (e.g., Megaw, 1968). Indeed, whereas refined site scattering (Table 7) suggested the replacement of Ti^{4+} by Fe in the sample from Monte Arsiccio, Moore and Araki (1976) reported a pure Ti occupancy for their sample. This effect is more clear at the *M*(3) and *M*(4) sites, having a mixed Ti/Fe^{3+} occupancy, and showing Δ*d* values of 0.285 and 0.301 Å, respectively. The lower degree of distortion shown by *M*(1) suggests that minor V^{3+} (having an atomic number *Z* similar to that of Ti, i.e., 23 *vs* 22) may be located at this site. The *M*(2)-centred octahedron has a pure Fe occupancy. The average bond distance (2.052 Å), as well as the bond-valence

calculations (Table 8), suggest the mixed Fe^{2+}/Fe^{3+} occupancy at this site. Considering the average bond distance and the ionic radii of Fe^{2+} and Fe^{3+} in octahedral coordination, using the values given by Shannon (1976), an idealized site population of $(Fe^{3+}_{0.65}Fe^{2+}_{0.35})$ may be proposed. The total site scattering observed at the *M*(1)-*M*(4) sites is 169.8 electrons per formula unit (epfu), comparable with 166.6 epfu calculated on the basis of electron microprobe data.

Mössbauer spectroscopy indicated that ferric and ferrous iron are both octahedrally coordinated. Again, the half-band widths of the fitted quadrupole doublets indicate that Fe is located in more than one polyhedron each, but that the mean M–O distances and distortions are fairly similar. This contrasts with the higher distortion degree of *M*(3) and *M*(4) sites with respect to *M*(1) and *M*(2). However, it is likely that the distortion is due to Ti^{4+}, whereas when these sites are occupied by Fe a more regular coordination occurs.

Cuboctahedral cavities host partially filled Sb(a), Sb(b), and Ba sites. Moore and Araki (1976) found only a fully occupied Sb site [i.e., Sb(a)], with average bond distance of 2.007 Å. On the contrary, the refinement of the crystal structure of the sample from Monte Arsiccio suggested the occurrence of two different Sb sites, Sb(a) and Sb(b). The former is preferentially occupied with respect to the latter. Since bond distances do not suggest any preferential partitioning of Sb and As within one out of the two sites, these two elements were equally partitioned among Sb(a) and Sb(b) sites. Considering the refined site scattering at the two positions, the site population $Sb_{0.63}As_{0.17}$ and $Sb_{0.13}As_{0.04}$ are proposed for Sb(a) and Sb(b), respectively. The discrepancy between observed and theoretical BVS (Table 8) is likely due to the average nature of the ligand positions, related to the statistical occupancy of Sb and As between two different positions. The Ba site is located close to the center of the cuboctahedral cavities. It has a twelve-fold coordination, with average bond distance 2.906 Å.

Graeserite

Atomic coordinates, site occupancies, and equivalent isotropic displacement parameters of the two samples of graeserite are given in Table 9, whereas selected bond distances are reported in Table 10.

The octahedral framework is formed by three independent *M*(1)–*M*(3) sites, whereas some partially filled sites occur in the cuboctahedral cavities. The *M*(1) octahedron is quite regular, with average bond distance of 1.981 Å (range 1.971 – 1.986 Å) and 1.972 Å (range 1.955 – 1.980 Å) for samples F and G, respectively. These values can be compared with the average distance reported by Berlepsch and Armbruster (1998), i.e., 1.984 Å. The distortion of this site is low, and comparable to that observed in derbylite. The *M*(2) site is the largest among octahedral sites and it has a mixed occupancy. Table 11 reports the proposed site population based on refined site scattering, electron microprobe data, and average bond distances. In both samples, a mixed (Ti,Me^{3+},Fe^{2+}) occupancy was proposed, with Me^{3+} = V and Fe in samples F and G, respectively. *M*(2) is distorted, with Δd values of 0.238 and 0.252 Å for samples F and G. This distortion is comparable with that shown by the site *M*(3), i.e. 0.232 and 0.213 Å for samples F and G, respectively. BVS at the *M*(1)-*M*(3) site agree with the theoretical values (Table 12). The total site scattering observed at the *M*(1)-*M*(3) sites is 158.0 and 164.4 epfu for samples F and G, to be compared with 165.4 and 167.4 epfu calculated on the basis of electron microprobe data.

As in derbylite, Mössbauer spectroscopy indicated that ferric and ferrous iron are both octahedrally coordinated in graeserite. Similarly, the half-band widths of the fitted quadrupole doublets are rather high, indicating that Fe is located in more than one polyhedron each, but that the mean M–O distances and distortions are fairly similar.

Berlepsch and Armbruster (1998) reported the occurrence of an As and a Pb site within the cuboctahedral cavities of Pb-bearing graeserite. In samples F and G some differences can be observed. Sample F has significant Sb replacing As. Antimony forms longer distances with O than As and the crystal structure refinement showed the possible splitting of the As site into two sub-positions. One, more populated, has shorter distances and it is compatible with an As occupancy, with possibly a very minor replacement of Sb; the other has a lower occupancy and longer distances and it is interpreted as an Sb position. In sample G, As is strongly dominant over Sb and only one site was modelled. In both cases, the statistical nature of these positions results in longer than ideal average distances (Table 11). For instance, in sample G, having a nearly pure As occupancy, an average distance of 1.846 Å has been observed, definitely longer than the average As^{3+}–O distance of 1.782 Å reported by Majzlan *et al*. (2014). Longer than ideal distances are reported in other related minerals like tomichite and the arsenite-antimonite mineral hemloite, $(Ti,V,Fe,Al)_{12}(As,Sb)_2O_{23}(OH)$ (Grey *et al*., 1987; Harris *et al*., 1989). Both samples contain Ba in detectable amounts, and sample G shows also the presence of minor Pb. Barium is twelve-four coordinated and occurs close to or at the center of the cuboctahedral cavities in samples F and G, respectively. On the contrary, sample G contains some Pb that was located in a site displaced from the center, likely due to the lone-electron-pair activity of Pb^{2+}. Its coordination is formed by five oxygen atoms, with distances shorter than 3 Å, and six additional longer bonds, between 3.09 and 3.18 Å, in agreement with Berlepsch and Armbruster (1998).

Metal partitioning among *M* sites

Taking into account the site multiplicity, the structural formula of derbylite and graeserite can be written (neglecting low-populated Ba/Pb sites) as $M(1)M(2)_2M(3)_2M(4)_2SbO_{13}(OH)$ (Z = 2) and $M(1)M(2)_2M(3)_4AsO_{12}[O_{0.5}(OH)_{0.5}]_2$ (Z = 2), respectively.

Titanium (Z = 22), V (Z = 23), and Fe (Z = 26) have similar scattering factors and their accurate partitioning among the *M* sites of derbylite and graeserite is not an easy task. In addition, ionic radii of these transition elements in six-fold coordination are very similar. Following Shannon (1976), the ionic radii are: Ti 0.605 Å, V^{3+} 0.640 Å, Fe^{3+} 0.645 Å, and Fe^{2+} 0.78 Å. Only Fe^{2+} is significantly larger than the other cations.

In derbylite, the largest site is *M*(2) and Fe^{2+} is likely hosted at this position. *M*(1), *M*(3), and *M*(4) have similar average bond distances. *M*(1) is likely a mixed (Ti,Fe,V) site, whereas *M*(3) and *M*(4) are mixed (Ti,Fe) site, with a higher Ti/Fe atomic ratio than that reported by Moore and Araki (1976), close to 1. The occurrence of $(Fe,V)^{3+}$ at *M*(1) and the different Ti/Fe ratios at *M*(3) and *M*(4) with respect to the results of Moore and Araki (1976) may be related to the cross-substitution ${}^{M(1)}Ti^{4+} + {}^{M(3),M(4)}Fe^{3+} = {}^{M(1)}(Fe,V)^{3+} + {}^{M(3),M(4)}Ti^{4+}$, as well as to the substitution ${}^{M(2)}Fe^{3+} + {}^{M(3),M(4)}Fe^{3+} = {}^{M(2)}Fe^{2+} + {}^{M(3),M(4)}Ti^{4+}$. The cation sites of derbylite from Monte Arsiccio give the following formula: ${}^{M(1)}(Ti_{0.5}Fe^{3+}_{0.3}V^{3+}_{0.2})^{M(2)}(Fe^{3+}_{0.65}Fe^{2+}_{0.35})_2{}^{M(3)}(Ti_{0.8}Fe^{3+}_{0.2})_2{}^{M(4)}(Ti_{0.8}Fe^{3+}_{0.2})_2$. This can be

compared with the formula proposed by Moore and Araki (1976), i.e., $^{M(1)}Ti^{M(2)}Fe^{3+}{}_2{}^{M(3)}(Ti_{0.57}Fe^{3+}{}_{0.43})_2{}^{M(4)}(Ti_{0.43}Fe^{3+}{}_{0.57})_2$. Applying the two substitution mechanisms described above, the structural formula of the Monte Arsiccio sample can be simplified as $^{M(1)}Ti^{M(2)}Fe^{3+}{}_2{}^{M(3),M(4)}(Ti_{0.5}Fe^{3+}{}_{0.5})_4$. The *M*(3) and *M*(4) sites are virtually indistinguishable and can be considered as an aggregate site.

In graeserite, the *M*(1) site is likely a mixed (Ti,Me^{3+}) site. In sample F, the refined site scattering at *M*(1) suggested a pure Ti occupancy. This is unlikely, because observed bond-length suggested the occurrence of a larger cation replacing Ti. In Table 11, a site population with a mixed ($Ti_{0.80}Fe^{3+}{}_{0.20}$) population is proposed. However, another possibility is represented by the occurrence of V^{3+} at this position. Vanadium has a scattering power very similar to that of Ti, and this could explain the observed site scattering; in addition, its ionic radius is similar to that of Fe^{3+}. Consequently, an alternative site population may be proposed for the *M*(1) and *M*(2) sites: $^{M(1)}(Ti_{0.60}V^{3+}{}_{0.40})$ and $^{M(2)}(Ti_{0.45}V^{3+}{}_{0.10}Fe^{3+}{}_{0.10}Fe^{2+}{}_{0.35})$, resulting in a calculated site scattering of 22.4 and 23.9 electrons, and calculated <*Me*–O> distances of 1.98 and 2.03 Å, respectively. These values are very similar to that reported in Table 11 for a slightly different cation distribution, indicating that a reliable metal partitioning among *M* sites can be very difficult. In the V-poor sample G, mixed (Ti,Fe^{3+}) and (Ti,Fe^{3+},Fe^{2+}) populations at the *M*(1) and *M*(2) sites have been proposed. In both samples F and G, the *M*(3) site is a mixed (Ti,Fe^{3+}) site, with a Ti/Fe atomic ratio close to 0.5. The *M*(1)-*M*(3) sites give the formulae $^{M(1)}(Ti_{0.80}Fe^{3+}{}_{0.20})^{M(2)}(Ti_{0.35}V^{3+}{}_{0.30}Fe^{2+}{}_{0.35})_2{}^{M(3)}(Ti_{0.55}Fe^{3+}{}_{0.45})_4$ and $^{M(1)}(Ti_{0.85}Fe^{3+}{}_{0.15})^{M(2)}(Ti_{0.50}Fe^{3+}{}_{0.20}Fe^{2+}{}_{0.30})_2{}^{M(3)}(Ti_{0.45}Fe^{3+}{}_{0.55})_4$ for samples F and G, respectively. Also in these cases the same substitutions proposed above can be applied, in addition to the substitution $V^{3+} = Fe^{3+}$. In both cases the formula approaches the composition $^{M(1)}Ti^{M(2)}Fe^{3+}{}_2{}^{M(3),M(4)}(Ti_{0.5}Fe^{3+}{}_{0.5})_4$.

In both derbylite and graeserite, the V_3O_5-type columns seems to have the more complex crystal-chemistry. Indeed, whereas its ideal cation composition is $TiFe^{3+}{}_2$, the actual chemistry is more complex, showing the occurrence of V^{3+} and Fe^{2+}. On the contrary, the α-PbO_2-type octahedral chains have a mixed (Ti,Fe) composition, with an ideal atomic ratio close to 1.

Hydroxyl group position and its relations with the cavity contents

The occurrence of OH groups in derbylite-related minerals has been assumed by several authors (e.g., Nickel and Grey, 1979; Mellini *et al*., 1983; Grey *et al*., 1987) on the basis of the structure solution of Moore and Araki (1976) but direct measurements of H_2O have not been reported yet. Grey *et al*. (1987) performed infrared spectroscopy and thermogravimetric analysis to confirm the occurrence of OH groups in barian tomichite. Both analyses were inconclusive, the former owing to the weakness and broadness of the stretching bands of O–H bonds observed around 3400 cm^{-1}, whereas the latter suffered the interference between the H_2O loss and the As volatilization. The most convincing data supporting the occurrence of OH groups are related to the solution and refinement of the crystal structures of derbylite-related minerals.

The examination of the BVS at the anion sites in derbylite from Monte Arsiccio (Table 8) shows the occurrence of a strongly underbonded anion, OH(8), having a BVS of 1.06 v.u. Since F is below the detection limit, this is the likely position of the OH group, in agreement

with Moore and Araki (1976). Actually, this is the most frequent configuration and it is related to the occupancy of the Sb(a) position. When Sb(a) is vacant and Sb(b) is occupied, the likely position of OH group is at the O(1) site that becomes underbonded. In both cases, O···O distances compatible with H-bonds are formed with two O(4) sites, with OH(8)···O(4) and O(1)···O(4) of 2.983(3) and 2.875(3) Å, respectively.

In graeserite, the location of OH groups is not straightforward. Table 12 shows that the weighted BVS at the O sites do not show any significant underbonding for the O atoms; the underbonding of O(4) is not so large to allow the proposal of the occurrence of OH groups at this position. However, a critical examination of these values is mandatory, in particular as regards the O(4) and O(5) sites. Indeed, the disordered nature of the sites occurring in the cuboctahedral cavities give rise to different local configurations, as exemplified in Figure 5. It is worth noting that O(4), shared between consecutive cuboctahedral cavities, can be bonded to only one As^{3+} cation, in order to avoid its overbonding. The possible occupancy at the cuboctahedral cavities has been discussed by Grey *et al*. (1987) and Berlepsch and Armbruster (1998). Whereas only one SbO_3 group can be hosted within a cuboctahedral cavity, owing to steric reasons, one or two AsO_3 groups can occupy one cavity. This is in agreement with the sum of (Ba/Pb) + (As/Sb) exceeding 1 apfu in As-dominant derbylite-related minerals.

Oxygen atoms hosted at O(4) and O(5) are bonded to two *M*(3) sites and to one *M*(1) and two *M*(2) sites, respectively. In this way, the resulting BVS at O(4) and O(5) are ~ 0.9 and 1.3-1.4 v.u., respectively. The actual BVS is then the result of the cation configuration in the cavities. There are three main possibilities (Fig. 5):

i) only one $(As/Sb)O_3$ group occurs within a cavity;
ii) two AsO_3 groups occur within a cavity;
iii) a (Ba/Pb) cation occurs in the cavity.

The first case is observed in derbylite. In this case, whereas O(4) is bonded to (As/Sb) atoms, achieving a BVS close to 2 v.u., the two O(5) sites can be divided in one bonded to the (As/Sb) atoms and the other that is not bonded. In the former case, O(5) achieves a total BVS close to 2 v.u. and it is occupied by an O^{2-} atom, whereas in the latter its BVS agrees with its occupancy by an OH group. In the second configuration, both O(4) and O(5) are always occupied by O^{2-}, whereas in the third configuration, O(5) is occupied by OH groups. It is worth noting that the configuration ii) and iii) are closely related, because they allow the electrostatic neutrality of the chemical formula, through the substitution $As^{3+} + {}^{O(5)}O^{2-} = (Ba/Pb)^{2+} + {}^{O(5)}OH^-$. This mechanism has been proposed above, during the discussion of the chemical formula of derbylite and graeserite and it is supported by bond-valence arguments. The other mechanism, $(As/Sb)^{3+} + 3O^{2-} = \square + 3OH^-$, seems to play a very minor role in derbylite-related minerals and it will not be discussed here.

It is worth noting that the occurrence of (Ba/Pb) atoms could also be considered as a kind of "structural defects" favouring a change in the "polarity" of the $(As/Sb)O_3$ trigonal pyramids. Indeed, two (AsO_3) groups can decorate a (Ba/Pb)-filled cavity (Fig. 5a) or only one (AsO_3) group can be bonded to an edge of the cuboctahedral cavity, in this way allowing the change of the direction of the lone-electron-pairs of (As/Sb) atoms (Fig. 5b). In this way, the O(4) sites not-bonded to (As/Sb) atoms are likely occupied by OH^-. As a final

consideration, it cannot be excluded that the local ordering could influence also the occupancy of nearby octahedral sites, adding further complexity to the real structure of graeserite.

Conclusion

The crystal-chemical characterization of derbylite and graeserite is a further puzzle tile in the mineralogical knowledge of the hydrothermal ores from the Apuan Alps. Subtle variations in the As/Sb ratio in the crystallization environments may favour the formation of derbylite (high Sb, low As) or graeserite (high As, low Sb). The role of Ba and minor Pb in the stabilization of the latter mineral is not clear. However, it seems likely that the crystal structure of graeserite can be a host for minor large divalent cations (e.g., Ba^{2+}, Pb^{2+}). The complex crystal-chemistry of the extraframework constituents (Sb, As, Ba, Pb) is likely at the origin of the satellite reflections reported by previous authors (e.g., Grey *et al*., 1987; Berlepsch and Armbruster, 1998) and the transition from the $P2_1/m$ to the $C2/m$ space group, as suggested by the pair tomichite – barian tomichite (Grey *et al*., 1987). Berlepsch and Armbruster (1998) attributed to the occurrence of incommensurate superstructure the presence of several residuals that were interpreted as disordered *M* sites. No such a kind of disorder was observed in the samples from the Monte Arsiccio mine, whereas some disorder was reported for sites hosted in the cuboctahedral cavities, as discussed above. This demands for further investigation to unravel the short-range cation order within these cuboctahedral cavities.

In addition to the finding of derbylite and graeserite in hydrothermal veins, the finding of graeserite as porphyroblast in schist from the Sant'Anna level suggests that this mineral may also occur as a metamorphic accessory phase in As-bearing environments. Its role in the possible release of As in the environment upon rock weathering is currently to be further investigated.

Acknowledgements

Alois Lechner is thanked for providing us with the specimen of graeserite from the Sant'Anna level. This research was financially supported by the Ministero dell'Istruzione, Università e Ricerca through the project PRIN 2017 "TEOREM – deciphering geological processes using Terrestrial and Extraterrestrial ORE Minerals", prot. 2017AK8C32, and from the University of Pisa through the project P.R.A. 2018-2019 "Georisorse e Ambiente" (Grant No. PRA_2018_41). The authors are grateful to the University Centrum for Applied Geosciences (UCAG) for the access to the E. F. Stumpfl electron microprobe laboratory. The careful revision of Yves Moëlo and two anonymous reviewers improved the manuscript.

References

Berlepsch, P. and Armbruster, T. (1998) The crystal structure of Pb^{2+}-bearing graeserite, $Pb_{0.14}(Fe,Ti)_7AsO_{12+x}(OH)_{2-x}$, a mineral of the derbylite group. *Schweizerische Mineralogische und Petrographische Mitteilungen*, **78**, 1-9.

Biagioni, C., Pasero, M., Hålenius, U. and Bosi, F. (2019) Bianchiniite, IMA 2019-022. CNMNC Newsletter No. 50. *Mineralogical Magazine*, 83, 615-620.

Brese, N.E. and O'Keeffe, M. (1991) Bond-valence parameters for solids. *Acta Crystallographica*, **B47**, 192-197.

Bruker AXS Inc. (2016) APEX 3. Bruker Advanced X-ray Solutions, Madison, Wisconsin, USA.

Grey, I.E., Madsen, I.C. and Harris, D.C. (1987) Barian tomichite, $Ba_{0.5}(As_2)_{0.5}Ti_2(V,Fe)_5O_{13}(OH)$, its crystal structure and relationship to derbylite and tomichite. *American Mineralogist*, **72**, 201-208.

Harris, D.C., Hoskins, B.F., Grey, I.E., Criddle, A.J. and Stanley, C.J. (1989) Hemloite, $(As,Sb)_2(Ti,V,Fe,Al)_{12}O_{23}OH$: a new mineral from the Hemlo gold deposit, Hemlo, Ontario, and its crystal structure. *Canadian Mineralogist*, **27**, 427-440.

Hussak, E. and Prior, G.T. (1895) Lewisite and zirkelite, two new Brazilian minerals. *Mineralogical Magazine*, **11**, 80-88.

Hussak, E. and Prior, G.T. (1897) On derbylite, a new antimono-titanate of iron, from Tripuhy, Brazil. *Mineralogical Magazine*, **11**, 176-179.

Krivovichev, S.V. (2012) Derivation of bond-valence parameters for some cation-oxygen pairs on the basis of empirical relationships between r_0 and b. *Zeitschrift für Kristallographie*, **227**, 575-579.

Krzeminicki, M.S. and Reusser, E. (1996) Graeserite, $Fe_4Ti_3AsO_{13}(OH)$, a new mineral species of the derbylite group from the Monte Leone Nappe, Binntal region, Western Alps, Switzerland. *Canadian Mineralogist*, **36**, 1083-1088.

Majzlan, J., Drahota, P. and Filippi, M. (2014) Parageneses and crystal chemistry of arsenic minerals. *Reviews in Mineralogy and Geochemistry*, **79**, 17-184.

Megaw, H.D. (1968) A simple theory of the off centre displacement of cations in octahedral environments. *Acta Crystallographica*, **B24**, 149-153.

Mellini, M., Orlandi, P. and Perchiazzi, N. (1983) Derbylite from Buca della Vena mine, Apuan Alps, Italy. *Canadian Mineralogist*, **21**, 513-516.

Mellini, M., Orlandi, P. and Vezzalini, G. (1986) V-bearing derbylite from the Buca della Vena mine, Apuan Alps, Italy. *Mineralogical Magazine*, **50**, 328-330.

Mills, S.J., Christy, A.G., Chen, E.C.-C. and Raudsepp, M. (2009) Revised values of the bond valence parameters for $^{[6]}$Sb(V)–O and $^{[3\text{-}11]}$Sb(III)–O. *Zeitschrift für Kristallographie*, 224, 423-431.

Moëlo, Y., Makovicky, E., Mozgova, N.N., Jambor, J.L., Cook, N., Pring., A., Paar, W.H., Nickel, E.H., Graeser, S., Karup-Møller, S., Balić-Žunić, T., Mumme, W.G., Vurro, F., Topa, D., Bindi, L., Bente, K. and Shimizu, M. (2008) Sulfosalt systematics: a review. Report of the sulfosalt sub-committee of the IMA Commission on Ore Mineralogy. *European Journal of Mineralogy*, **20**, 7–46.

Nickel, E.H. and Grey, I.E. (1979) Tomichite, a new oxide mineral from Western Australia. *Mineralogical Magazine*, **43**, 469-471.

Moore, P.B. and Araki, T. (1976) Derbylite, $Fe_4^{3+}Ti_3^{4+}Sb^{3+}O_{13}(OH)$, a novel close-packed oxide structure. *Neues Jahrbuch für Mineralogie Abhandlungen*, **126**, 292-303.

Prescher, C., McCammon, C. and Dubrovinsky, L. (2012) MossaA: a program for analyzing energy-domain Mössbauer spectra from conventional and synchrotron sources. *Journal of Applied Crystallography*, **45**, 329–331.

Shannon, R.D. (1976) Revised effective ionic radii and systematic studies of interatomic distances in halides and chalcogenides. *Acta Crystallographica*, **A32**, 751-767.

Sheldrick, G.M. (2015) Crystal structure refinement with SHELXL. *Acta Crystallographica*, **C71**, 3–8.

Wilson, A.J.C., Ed. (1992) *International Tables for X-ray Crystallography*, Volume C: Mathematical, physical and chemical tables. Kluwer Academic, Dordrecht, NL.

Table captions

Table 1. Studied samples of derbylite (A-D) and graeserite (E-G).

Table 2. Chemical composition (in wt%) and chemical formulae (in atoms per formula unit, apfu, on the basis of Ti + V + Cr + Fe = 7 apfu) of derbylite (A-D) and graeserite (E-G) samples from the Monte Arsiccio mine.

Table 3. Hyperfine parameters for fitted doublets in the Mössbauer spectra of derbylite (sample C) and graeserite (sample F).

Table 4. Crystal data and summary of parameters describing data collection and refinement for derbylite and graeserite.

Table 5. Atomic coordinates, site occupation factors, and equivalent isotropic or isotropic (*) displacement parameters ($Å^2$) for derbylite.

Table 6. Selected bond-distances (in Å) for derbylite.

Table 7. Refined site scattering *vs*. calculated site scattering (in electrons), proposed site population, observed and calculated average distances (Å) for derbylite.

Table 8. Bond valence sums (BVS – in valence unit, *v.u.*) for derbylite.

Table 9. Atomic coordinates, site occupation factors, and equivalent isotropic or isotropic (*) displacement parameters ($Å^2$) for graeserite.

Table 10. Selected bond-distances (in Å) for derbylite.

Table 11. Refined site scattering *vs*. calculated site scattering (in electrons), proposed site population, observed and calculated average distances (Å) for graeserite.

Table 12. Bond valence sums (BVS – in valence unit, *v.u.*) for graeserite.

Figure captions

Fig. 1. Selected samples of derbylite and graeserite from the Monte Arsiccio mine. (a) Black prismatic crystal of derbylite, deeply striated, with siderite, baryte, and "hyalophane". (b) Black acicular crystal of derbylite with magnetite, siderite, "hyalophane", and quartz. (c) Aggregate of prismatic crystals of graeserite grown on ankerite. (d) Twinned crystals of graeserite with "hyalophane", dolomite, and siderite.

Fig. 2. Mössbauer spectra of derbylite (upper) and graeserite (lower).

Fig. 3. Chemical variability in derbylite (light blue diamonds) and graeserite (red triangles) samples from the Monte Arsiccio mine.

Fig. 4. The octahedral framework characterizing derbylite and graeserite, as seen down **a** (a) and its constitutive V_3O_5-type (b) and α-PbO_2-type (c) octahedral columns. The axial setting of graeserite was used.

Fig. 5. Hypothetical ordered sequences within the cuboctahedral cavities of graeserite. Symbols: large circle represents Ba, medium circle is As, and small circles are O sites. The O(5) site is highlighted and it is shown as light blue circles. For the sake of completeness, labels of the other O sites forming the cavities are shown in (a).

Table 1. Studied samples of derbylite (A-D) and graeserite (E-G).

Label	Occurrence	Description	Associated minerals
A	Siderite + baryte veins in magnetite-rich metadolostone	Black prismatic crystals, deeply striated	Baryte, boulangerite, galena, "hyalophane", siderite, stibivanite
B	Siderite + baryte veins in magnetite-rich metadolostone	Black thin acicular crystals	"Hyalophane", magnetite, quartz, siderite
C	Siderite + baryte veins in magnetite-rich metadolostone	Black acicular crystals	Baryte, "hyalophane", siderite
D	Siderite veins in magnetite-rich metadolostone	Black acicular crystals, striated	Limonitized iron carbonates, "hyalophane"
E	Ankerite ± baryte veins in pyrite-rich metadolostone	Black tabular prismatic crystals	Ankerite, arsenopyrite, baryte, "hyalophane", "tourmaline"
F	Dolomite + baryte ± siderite ± "hyalophane" veins in pyrite- ± magnetite-rich metadolostone	Black prismatic crystals, usually twinned	Ankerite, arsenopyrite, baryte, bianchiniite, dolomite, galena, "hyalophane", pyrite, quartz, rutile, siderite, sphalerite, stibivanite, "tourmaline"
G	Schist	Black twinned prismatic crystals	"Mica", quartz

Table 2. Chemical composition (in wt%) and chemical formulae (in atoms per formula unit, apfu, on the basis of Ti + V + Cr + Fe = 7 apfu) of derbylite (A-D) and graeserite (E-G) samples from the Monte Arsiccio mine.

Oxide	A (n = 15)	B (n = 4)	C (n = 10)	D (n = 15)	E (n = 15)	F (n = 14)	G (n = 15)
TiO_2	42.21(19)	39.71(80)	41.73(27)	42.37(25)	40.02(16)	42.06(39)	40.39(42)
V_2O_3	3.15(14)	1.63(10)	2.45(22)	2.20(17)	7.07(24)	6.08(26)	0.32(3)
Cr_2O_3	0.49(9)	n.a.	0.22(3)	0.36(7)	0.61(2)	0.52(3)	n.a.
FeO_{tot}	30.89(25)	31.16(41)	31.45(41)	30.99(35)	28.23(24)	27.88(22)	33.55(31)
Fe_2O_3	26.60	27.54	27.32	26.17	25.47	23.26	30.35
FeO	6.96	6.38	6.87	7.44	5.31	6.95	6.24
As_2O_3	3.72(11)	2.39(43)	2.97(25)	2.97(18)	8.95(31)	8.43(48)	11.99(38)
Sb_2O_3	14.71(20)	15.89(29)	15.68(18)	16.02(38)	5.93(49)	7.47(83)	1.48(12)
BaO	0.49(7)	n.a.	0.97(41)	0.69(54)	5.37(21)	4.25(41)	4.16(15)
PbO	0.23(9)	0.14(8)	0.11(5)	0.23(11)	0.31(11)	0.37(7)	2.64(18)
H_2O_{calc}	1.37	1.30	1.28	1.24	0.93	0.94	0.78
Total	99.93	94.98	99.60	99.69	99.97	100.33	98.35
apfu							
Ti^{4+}	3.67	3.65	3.67	3.73	3.52	3.68	3.62
V^{3+}	0.29	0.16	0.23	0.21	0.66	0.57	0.03
Cr^{3+}	0.04	-	0.02	0.03	0.06	0.05	-
Fe^{3+}	2.32	2.53	2.41	2.30	2.24	2.03	2.72
Fe^{2+}	0.67	0.65	0.67	0.73	0.52	0.68	0.62
As^{3+}	0.26	0.18	0.21	0.21	0.64	0.60	0.87
Sb^{3+}	0.70	0.80	0.76	0.77	0.29	0.36	0.07
Ba^{2+}	0.02	-	0.04	0.03	0.25	0.19	0.19
Pb^{2+}	0.01	0.00	0.00	0.01	0.01	0.01	0.08
O^{2-}	12.94	12.94	13.00	13.03	13.27	13.27	13.38
$(OH)^-$	1.06	1.06	1.00	0.97	0.73	0.73	0.62

n = number of spot analyses; n.a. = not analyzed.

Sample A: $Fe^{2+}_{0.67}(Fe^{3+}_{2.32}V_{0.29}Cr_{0.04})Ti_{3.67}[(Sb_{0.70}As_{0.26})(Ba_{0.02}Pb_{0.01})]O_{12.94}(OH)_{1.06}$

Sample B: $Fe^{2+}_{0.65}(Fe^{3+}_{2.53}V_{0.16})Ti_{3.65}[(Sb_{0.80}As_{0.18})]O_{12.94}(OH)_{1.06}$

Sample C: $Fe^{2+}_{0.67}(Fe^{3+}_{2.41}V_{0.23}Cr_{0.02})Ti_{3.67}[(Sb_{0.76}As_{0.21})(Ba_{0.04})]O_{13.00}(OH)_{1.00}$

Sample D: $Fe^{2+}_{0.73}(Fe^{3+}_{2.30}V_{0.21}Cr_{0.03})Ti_{3.73}[(Sb_{0.77}As_{0.21})(Ba_{0.03}Pb_{0.01})]O_{13.03}(OH)_{0.97}$

Sample E: $Fe^{2+}_{0.52}(Fe^{3+}_{2.24}V_{0.66}Cr_{0.06})Ti_{3.52}[(As_{0.64}Sb_{0.29})(Ba_{0.25}Pb_{0.01})]O_{13.27}(OH)_{0.73}$

Sample F: $Fe^{2+}_{0.68}(Fe^{3+}_{2.03}V_{0.57}Cr_{0.05})Ti_{3.68}[(As_{0.60}Sb_{0.36})(Ba_{0.19}Pb_{0.01})]O_{13.27}(OH)_{0.73}$

Sample G: $Fe^{2+}_{0.62}(Fe^{3+}_{2.72}V_{0.03})Ti_{3.62}[(As_{0.87}Sb_{0.07})(Ba_{0.19}Pb_{0.08})]O_{13.38}(OH)_{0.62}$

Table 3. Hyperfine parameters for fitted doublets in the Mössbauer spectra of derbylite (sample C) and graeserite (sample F).

	CS (mm/s)	QS (mm/s)	FWHM (mm/s)	Int(%)
Derbylite (Sample C)				
Fe^{3+}	0.42(2)	0.54(5)	0.48(1)	81(2)
Fe^{2+}	0.94(12)	1.58(24)	0.54(7)	19(2)
Graeserite (Sample F)				
Fe^{3+}	0.42(1)	0.56(1)	0.50(1)	79(2)
Fe^{2+}	1.05(3)	1.69(7)	0.56(6)	21(2)

Uncertainties within brackets. χ^2 = 1.43 and 1.92 for derbylite and graeserite, respectively.

Table 4. Crystal data and summary of parameters describing data collection and refinement for derbylite and graeserite.

Crystal data			
	Derbylite (sample C)	Graeserite (sample F)	Graeserite (sample G)
Crystal size (mm)	0.11 × 0.08 × 0.07	0.07 × 0.05 × 0.03	0.10 × 0.09 × 0.06
Cell setting, space group	Monoclinic, $P2_1/m$	Monoclinic, $C2/m$	Monoclinic, $C2/m$
a (Å)	7.1690(3)	5.0225(7)	5.0275(4)
b (Å)	14.3515(7)	14.3114(18)	14.2668(11)
c (Å)	4.9867(2)	7.1743(9)	7.1663(5)
β (°)	104.820(3)	104.878(3)	105.123(4)
V (Å^3)	495.99(4)	498.39(11)	496.21(7)
Z	2	2	2
Data collection and refinement			
Radiation, wavelength (Å)	Mo $K\alpha$, λ = 0.71073	Mo $K\alpha$, λ = 0.71073	Mo $K\alpha$, λ = 0.71073
Temperature (K)	293	293	293
$2\theta_{max}$	70.92	52.44	73.36
Measured reflections	7432	1361	3860
Unique reflections	2172	439	1125
Reflections with $F_o > 4\sigma(F_o)$	1955	428	1081
R_{int}	0.0230	0.0211	0.0157
$R\sigma$	0.0232	0.0208	0.0136
Range of h, k, l	$-11 \le h \le 11$, $-17 \le k \le 23$, $-7 \le l \le 8$	$-6 \le h \le 5$, $-13 \le k \le 17$, $-6 \le l \le 8$	$-8 \le h \le 7$, $-23 \le k \le 18$, $-9 \le l \le 12$
R [$F_o > 4\sigma(F_o)$]	0.0352	0.0399	0.0237
R (all data)	0.0402	0.0413	0.0246
wR (on F_o^2)	0.1113	0.0865	0.0611
Goof	1.156	1.288	1.111
Number of least-squares parameters	116	68	69
Maximum and minimum residual peak (e Å^{-3})	3.96 [at 0.56 Å from Sb(b)] -2.55 [at 0.00 Å from Sb(b)]	1.00 [at 0.90 Å from As] -0.85 [at 1.37 Å from O(4)]	2.50 [at 0.56 Å from Ba(2)] -2.03 [at 0.55 Å from As]

Table 5. Atomic coordinates, site occupation factors, and equivalent isotropic or isotropic (*) displacement parameters (Å^2) for derbylite.

Site	Wyckoff position	s.o.f.	*x*	*y*	*z*	$U_{eq/iso}$
M(1)	2*e*	$Fe_{0.68(1)}Ti_{0.32(1)}$	0.49648(8)	¼	0.74815(12)	0.00760(18)
M(2)	4*f*	$Fe_{1.00}$	0.50351(5)	0.13033(3)	0.24692(8)	0.00774(12)
M(3)	4*f*	$Ti_{0.70(1)}Fe_{0.30(1)}$	0.81023(7)	0.05935(3)	0.86972(10)	0.00704(14)
M(4)	4*f*	$Ti_{0.67(1)}Fe_{0.33(1)}$	0.81636(7)	-0.06277(3)	0.37392(10)	0.00719(14)
Sb(a)	2*e*	$Sb_{0.74(1)}$	0.07554(5)	¼	0.04451(9)	0.01080(11)
Sb(b)	2*e*	$As_{0.24(1)}$	0.9223(2)	¼	0.4569(4)	0.01080(11)
O(1)	2*e*	$O_{1.00}$	0.3468(4)	¼	0.0296(7)	0.0088(5)
O(2)	4*f*	$O_{1.00}$	0.6800(3)	-0.04488(15)	-0.0090(4)	0.0068(3)
O(3)	4*f*	$O_{1.00}$	0.6628(3)	0.15142(15)	-0.0297(5)	0.0089(4)
O(4)	4*f*	$O_{1.00}$	0.0014(3)	0.15077(17)	0.7598(4)	0.0092(4)
O(5)	4*f*	$O_{1.00}$	0.0004(2)	0.03653(16)	0.2507(4)	0.0059(4)
O(6)	4*f*	$O_{1.00}$	0.6821(3)	0.04397(15)	0.4884(4)	0.0072(4)
O(7)	4*f*	$O_{1.00}$	0.3342(3)	0.15141(15)	0.5183(5)	0.0088(4)
O(8)	2*e*	$O_{1.00}$	0.6437(4)	¼	0.4576(7)	0.0085(5)
Ba	2*e*	$Ba_{0.04(1)}$	0.0005(7)	¼	0.2475(11)	0.0114(18)*

Table 6. Selected bond-distances (in Å) for derbylite.

M(1)	– O(1)	1.973(3)	*M*(2)	– O(6)	1.959(2)	*M*(3)	– O(3)	1.840(2)
	– O(3)	1.994(2) ×2		– O(2)	1.961(2)		– O(6)	1.902(2)
	– O(7)	1.997(2) ×2		– O(3)	2.026(2)		– O(2)	1.940(2)
	– OH(8)	1.999(3)		– O(7)	2.058(2)		– O(5)	2.0615(18)
	Average	1.992		– OH(8)	2.1267(19)		– O(4)	2.070(2)
				– O(1)	2.183(2)		– O(5)	2.125(2)
				Average	2.052		average	1.990
M(4)	– O(7)	1.835(2)	Sb(a)	– O(1)	1.965(3)	Ba	– O(7)	2.810(5) ×2
	– O(2)	1.927(2)		– O(4)	1.985(2) ×2		– O(4)	2.820(5) ×2
	– O(6)	1.970(2)		Average	1.978		– O(3)	2.839(5) ×2
	– O(5)	2.0283(18)					– O(4)	2.924(5) ×2
	– O(4)	2.048(2)	Sb(b)	– OH(8)	1.998(3)		– O(1)	2.953(6)
	– O(5)	2.136(2)		– O(4)	2.048(3) ×2		– OH(8)	3.002(6)
	Average	1.990		Average	2.031		– O(5)	3.064(2) ×2
							average	2.906

Table 7. Refined site scattering *vs*. calculated site scattering (in electrons), proposed site population, observed and calculated average distances (Å) for derbylite.

Site	Refined site scattering	Proposed site population	Calculated site scattering	$<Me–O>_{obs}$	$<Me–O>_{calc}$
M(1)	24.7	$Ti_{0.5}Fe^{3+}_{0.3}V_{0.2}$	23.4	1.992	1.98
M(2)	26.0	$Fe^{3+}_{0.65}Fe^{2+}_{0.35}$	26.0	2.052	2.05
M(3)	23.2	$Ti_{0.8}Fe^{3+}_{0.2}$	22.8	1.990	1.98
M(4)	23.3	$Ti_{0.8}Fe^{3+}_{0.2}$	22.8	1.990	1.98
Sb(a)	37.7	$Sb_{0.63}As_{0.17}\square_{0.19}$	37.7	1.978	1.90
Sb(b)	7.9	$\square_{0.82}Sb_{0.13}As_{0.04}$	7.9	2.031	1.90
Ba	2.2	$\square_{0.96}Ba_{0.04}$	2.2	2.906	2.97

Note: average <*Me*–O> distances for *M*(1)-*M*(4) and Ba sites have been calculated using the ionic radii given by Shannon (1976) and the bond parameters of Brese and O'Keeffe (1991) and Mills *et al*. (2009) for As and Sb. For the partially occupied sites, a full-occupancy is assumed for calculating the ideal <*Me*–O> distances.

Table 8. Weighted bond valence sums (BVS – in valence unit, *v.u.*) for derbylite.

Site	O(1)	O(2)	O(3)	O(4)	O(5)	O(6)	O(7)	OH(8)	∑cations	Theor.
M(1)	0.60		$^{2\times\rightarrow}$0.57				$^{2\times\rightarrow}$0.56	0.56	3.42	3.50
M(2)	0.31$^{\downarrow\times2}$	0.57	0.47			0.57	0.44	0.36	2.72	2.65
M(3)		0.69	0.91	0.49	0.50 0.42	0.77			3.78	3.80
M(4)		0.72		0.52	0.55 0.41	0.64	0.92		3.76	3.80
Sb(a)	0.68			$^{2\times\rightarrow}$0.65					1.98	2.40
Sb(b)				$^{2\times\rightarrow}$0.12				0.13	0.37	0.51
Ba	0.01		$^{2\times\rightarrow}$0.01	$^{2\times\rightarrow}$0.01 $^{2\times\rightarrow}$0.01			$^{2\times\rightarrow}$0.01	0.01	0.10	0.08
∑anions	1.91	1.98	1.96	1.79	1.88	1.98	1.93	1.06		
Theor.	2.00	2.00	2.00	2.00	2.00	2.00	2.00	1.00		

Table 9. Atomic coordinates, site occupation factors, and equivalent isotropic or isotropic (*) displacement parameters (Å^2) for graeserite.

Site	Wyckoff position	s.o.f.	*x*	*y*	*z*	$U_{eq/iso}$
Sample F						
M(1)	2*d*	$Ti_{1.00}$	0	½	½	0.0102(8)
M(2)	4*g*	$Ti_{0.71(4)}Fe_{0.29(4)}$	-½	0.61918(13)	½	0.0086(6)
M(3)	8*j*	$Ti_{0.91(4)}Fe_{0.09(4)}$	-0.3810(3)	0.80959(9)	0.81403(17)	0.0087(5)
As	4*i*	$As_{0.69(1)}$	-0.252(4)	½	0.914(3)	0.012(2)
Sb	4*i*	$Sb_{0.31(1)}$	-0.306(7)	½	0.930(5)	0.012(2)
O(1)	8*j*	$O_{1.00}$	-0.2712(11)	0.9021(4)	0.6618(8)	0.0157(13)
O(2)	8*j*	$O_{1.00}$	-0.2674(10)	0.7034(4)	0.6785(7)	0.0141(13)
O(3)	4*h*	$O_{1.00}$	-½	0.7122(5)	0	0.0120(17)
O(4)	4*h*	$O_{1.00}$	-½	0.9017(5)	0	0.0161(18)
O(5)	4*i*	$O_{1.00}$	-0.2801(16)	½	0.6486(11)	0.0172(19)
Ba	4*i*	$Ba_{0.23(1)}$	-0.493(3)	½	-0.0123(19)	0.0096(18)*
Sample G						
M(1)	2*d*	$Ti_{0.84(2)}Fe_{0.16(2)}$	0	½	½	0.01097(15)
M(2)	4*g*	$Ti_{0.58(2)}Fe_{0.42(2)}$	-½	0.61941(3)	½	0.00841(10)
M(3)	8*j*	$Ti_{0.59(2)}Fe_{0.41(2)}$	-0.37935(6)	0.80937(2)	0.81408(4)	0.00844(9)
As	4*i*	$As_{0.96(1)}Sb_{0.04(1)}$	-0.24326(12)	½	0.91447(7)	0.01147(17)
O(1)	8*j*	$O_{1.00}$	-0.2695(3)	0.90220(8)	0.66086(18)	0.0106(2)
O(2)	8*j*	$O_{1.00}$	-0.2676(3)	0.70296(9)	0.67771(18)	0.0107(2)
O(3)	4*h*	$O_{1.00}$	-½	0.71360(12)	0	0.0086(3)
O(4)	4*h*	$O_{1.00}$	-½	0.90412(13)	0	0.0144(4)
O(5)	4*i*	$O_{1.00}$	-0.2771(4)	½	0.6473(3)	0.0111(3)
Ba(1)	2*c*	$Ba_{0.25(1)}$	-½	½	0	0.0099(3)*
Ba(2)	4*i*	$Pb_{0.07(1)}$	-0.4583(6)	½	0.9395(5)	0.0220(9)*

Table 10. Selected bond-distances (in Å) for graeserite.

Sample F						Sample G					
M(1)	– O(5)	1.971(8) ×2	*M*(2)	– O(2)	1.921(6) ×2	*M*(1)	– O(5)	1.9552(18) ×2	*M*(2)	– O(2)	1.9056(13) ×2
	– O(1)	1.986(6) ×4		– O(1)	2.027(6) ×2		– O(1)	1.9803(12) ×4		– O(1)	2.0186(13) ×2
	Average	1.981		– O(5)	2.159(5) ×2		average	1.972		– O(5)	2.1577(12) ×2
				average	2.036					average	2.027
M(3)	– O(1)	1.887(6)	Ba	– O(1)	2.775(13) ×2	*M*(3)	– O(1)	1.8924(13)	Ba(1)	– O(1)	2.8233(13) ×4
	– O(2)	1.944(5)		– O(4)	2.829(12) ×2		– O(2)	1.9495(13)		– O(4)	2.8618(9) ×4
	– O(2)	1.966(6)		– O(1)	2.886(13) ×2		– O(2)	1.9651(13)		– O(5)	3.0201(17) ×2
	– O(3)	2.0562(17)		– O(5)	2.898(15)		– O(3)	2.0480(4)		– O(3)	3.0474(17) ×2
	– O(4)	2.070(5)		– O(4)	2.930(12) ×2		– O(4)	2.0958(12)		average	2.906
	– O(3)	2.119(5)		– O(3)	3.039(8 ×2)		– O(3)	2.1051(12)			
	Average	2.007		– O(5)	3.104(14)		average	2.009	Pb(2)	– O(5)	2.492(4)
				average	2.910					– O(1)	2.599(3) ×2
						As	– O(4)	1.8307(14 ×2)		– O(4)	2.617(3) ×2
As	– O(5)	1.87(2)	Sb	– O(4)	2.05(2) ×2		– O(5)	1.8773(18)		– O(3)	3.0930(18) ×2
	– O(4)	1.889(17) ×2		– O(5)	2.06(3)		average	1.846		– O(1)	3.122(3) ×2
	Average	1.88		average	2.05					– O(4)	3.177(3) ×2
										average	2.882

Table 11. Refined site scattering *vs*. calculated site scattering (in electrons), proposed site population, observed and calculated average distances (Å) for graeserite.

Site	Refined site scattering	Proposed site population	Calculated site scattering	$<Me–O>_{obs}$	$<Me–O>_{calc}$
Sample F					
M(1)	22.0	$Ti_{0.80}Fe^{3+}_{0.20}$	22.8	1.981	1.98
M(2)	23.2	$Ti_{0.35}V^{3+}_{0.30}Fe^{2+}_{0.35}$	23.7	2.036	2.04
M(3)	22.4	$Ti_{0.55}Fe^{3+}_{0.45}$	23.8	2.007	1.99
As	22.8	$As_{0.60}Sb_{0.05}\square_{0.35}$	22.4	1.88	1.80
Sb	15.8	$\square_{0.69}Sb_{0.31}$	15.8	2.05	1.92
Ba	12.9	$\square_{0.80}Ba_{0.19}Pb_{0.01}$	11.5	2.910	2.98
Sample G					
M(1)	22.6	$Ti_{0.85}Fe^{3+}_{0.15}$	22.6	1.972	1.98
M(2)	23.7	$Ti_{0.50}Fe^{3+}_{0.20}Fe^{2+}_{0.30}$	24.0	2.027	2.03
M(3)	23.6	$Ti_{0.45}Fe^{3+}_{0.55}$	24.2	2.009	2.00
As	33.7	$As_{0.87}Sb_{0.07}\square_{0.06}$	32.3	1.846	1.80
Ba(1)	14.0	$\square_{0.79}Ba_{0.19}Pb_{0.02}$	12.3	2.906	2.98
Pb(2)	5.7	$\square_{0.94}Pb_{0.06}$	4.9	2.882	2.82

Note: average <*Me*–O> distances for *M*(1)-*M*(3), Ba, and Pb sites have been calculated using the ionic radii given by Shannon (1976) and the bond parameters of Brese and O'Keeffe (1991) and Mills *et al*. (2009) for As and Sb. For the partially occupied sites, a full-occupancy is assumed for calculating the ideal <*Me*–O> distances.

Table 12. Weighted bond valence sums (BVS – in valence unit, *v.u.*) for graeserite.

Site	O(1)	O(2)	O(3)	O(4)	O(5)	∑cations	Theor.
Sample F							
M(1)	$^{3x\rightarrow}$0.61				$^{3x\rightarrow}$0.64	3.75	3.80
M(2)	$^{2x\rightarrow}$0.50	$^{2x\rightarrow}$0.66			$^{2x\rightarrow}$0.35$^{\downarrow\times2}$	3.02	3.00
M(3)	0.77	0.66 0.62	0.49$^{\downarrow\times2}$ 0.41$^{\downarrow\times2}$	0.47$^{\downarrow\times2}$		3.42	3.55
As				$^{2x\rightarrow}$0.51	0.54	1.56	1.95
Sb				$^{2x\rightarrow}$0.24	0.23	0.71	0.93
Ba	$^{2x\rightarrow}$0.05 $^{2x\rightarrow}$0.04		$^{2x\rightarrow}$0.03	$^{2x\rightarrow}$0.04 $^{2x\rightarrow}$0.03	0.04 0.02	0.44	0.40
∑anions	1.93/1.92	1.94	1.83	1.73/1.72	2.15/2.13		
Sample G							
M(1)	$^{3x\rightarrow}$0.63				$^{3x\rightarrow}$0.67	3.90	3.85
M(2)	$^{2x\rightarrow}$0.53	$^{2x\rightarrow}$0.71			$^{2x\rightarrow}$0.36$^{\downarrow\times2}$	3.20	3.20
M(3)	0.75	0.64 0.62	0.49$^{\downarrow\times2}$ 0.42$^{\downarrow\times2}$	0.43$^{\downarrow\times2}$		3.35	3.45
As				$^{2x\rightarrow}$0.74	0.78	2.26	2.82
Ba	$^{4x\rightarrow}$0.04		$^{2x\rightarrow}$0.02	$^{4x\rightarrow}$0.04	$^{2x\rightarrow}$0.03	0.50	0.40
Pb	$^{2x\rightarrow}$0.02 $^{2x\rightarrow}$0.01		$^{2x\rightarrow}$0.01	$^{2x\rightarrow}$0.02 $^{2x\rightarrow}$0.01	0.02	0.16	0.12
∑anions	1.97/1.96	1.97	1.85	1.66/1.65	2.20/2.22		

Fig. 1. Selected samples of derbylite and graeserite from the Monte Arsiccio mine. (a) Black prismatic crystal of derbylite, deeply striated, with siderite, baryte, and "hyalophane". (b) Black acicular crystal of derbylite with magnetite, siderite, "hyalophane", and quartz. (c) Aggregate of prismatic crystals of graeserite grown on ankerite. (d) Twinned crystals of graeserite with "hyalophane", dolomite, and siderite.

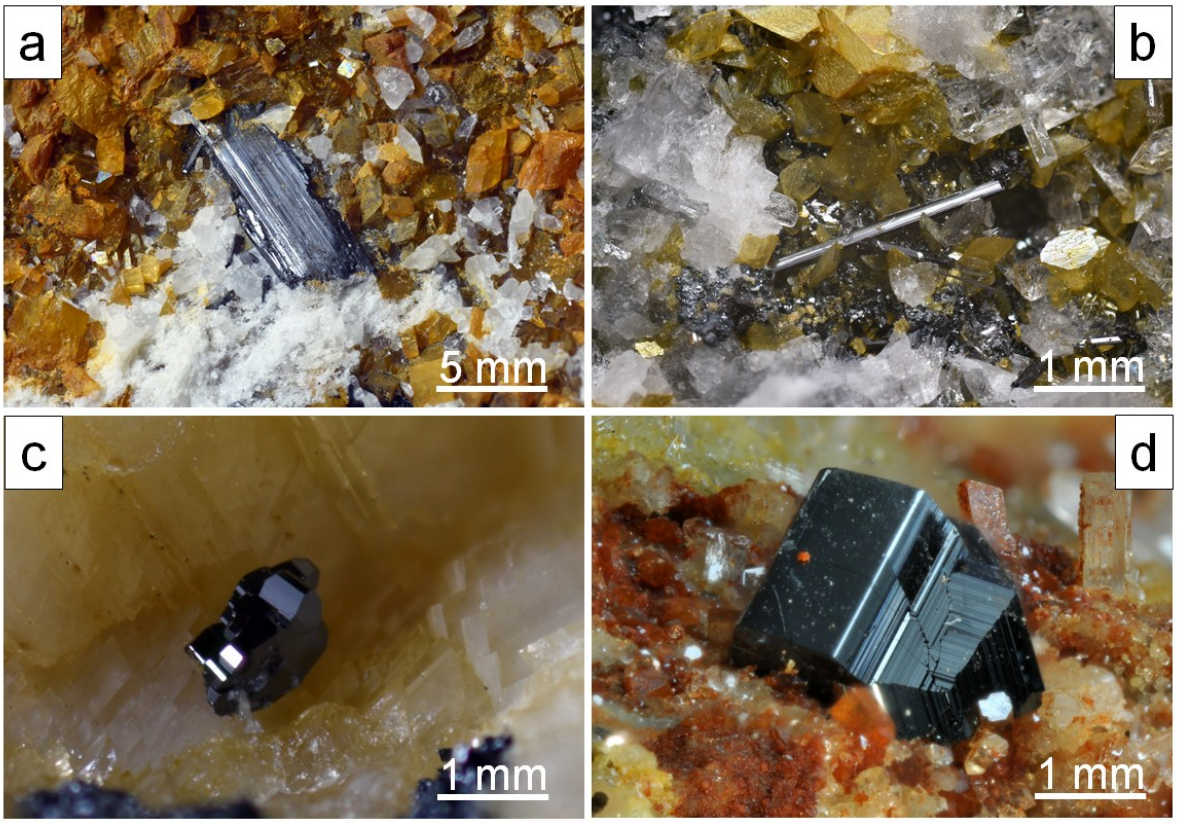

Fig. 2. Mössbauer spectra of derbylite (upper) and graeserite (lower).

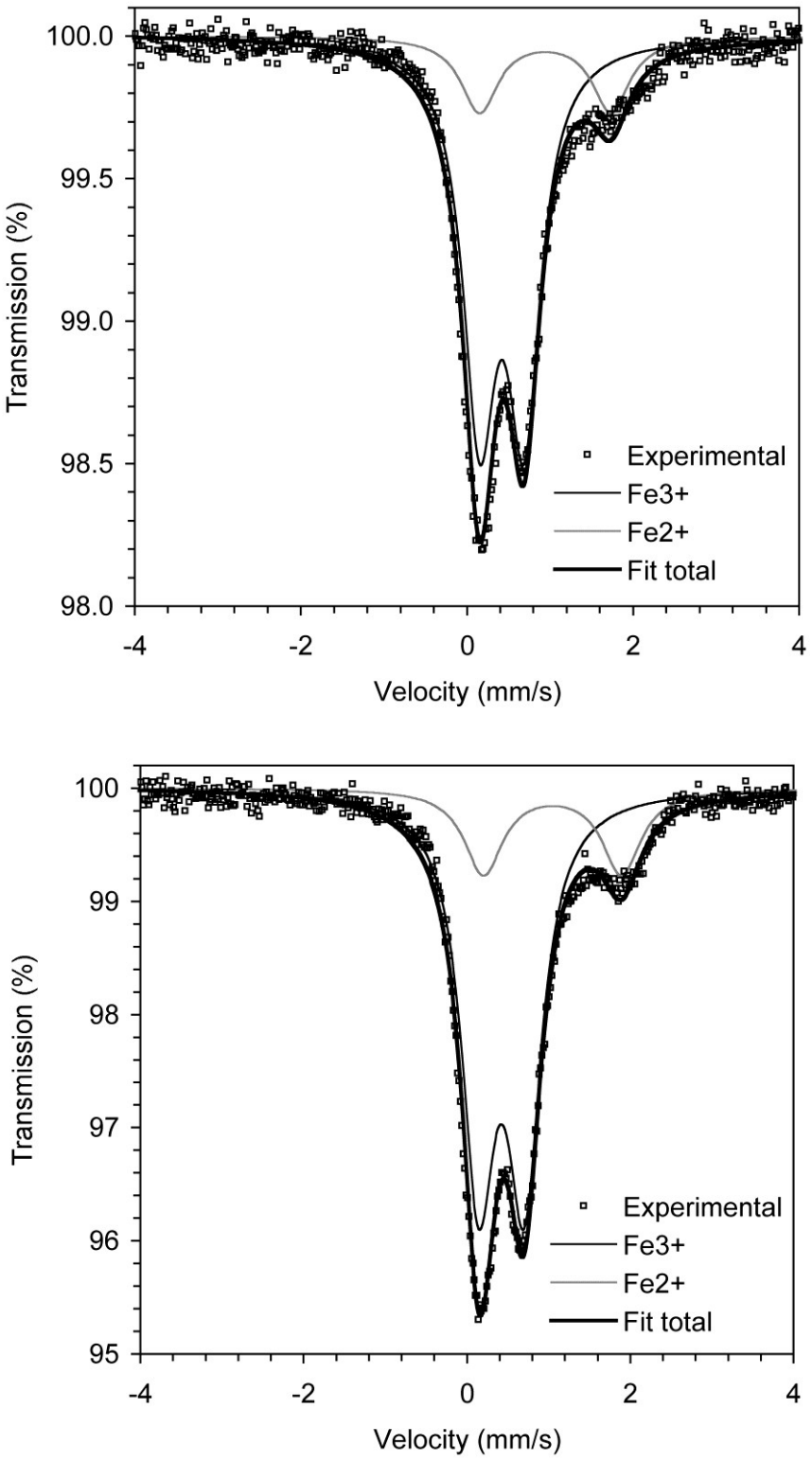

Fig. 3. Chemical variability in derbylite (light blue diamonds) and graeserite (red triangles) samples from the Monte Arsiccio mine.

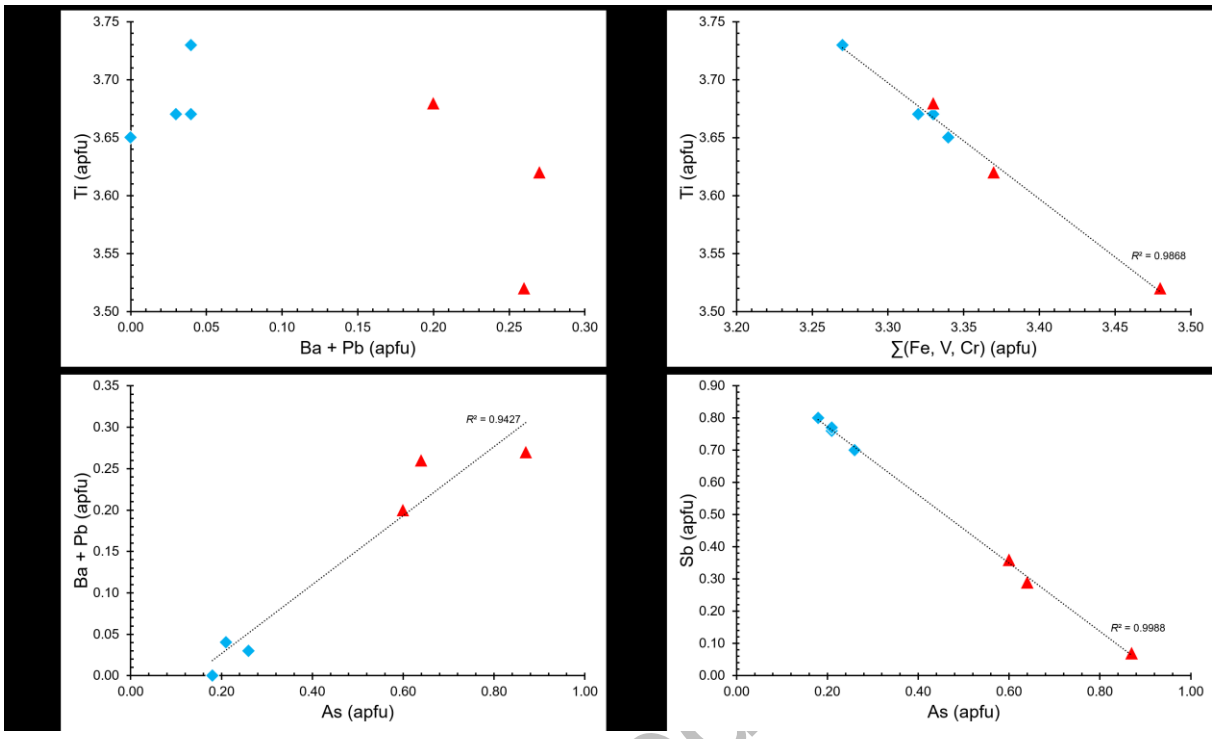

Fig. 4. The octahedral framework characterizing derbylite and graeserite, as seen down **a** (a) and its constitutive V_3O_5-type (b) and α-PbO_2-type (c) octahedral columns. The axial setting of graeserite was used.

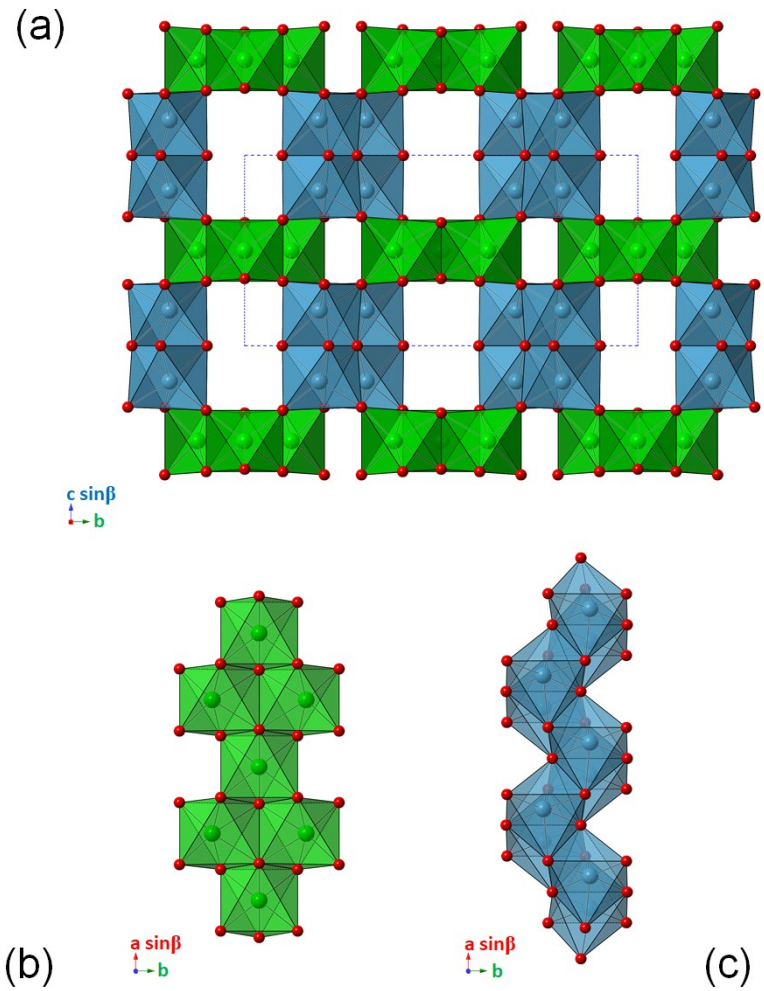

Fig. 5. Hypothetical ordered sequences within the cuboctahedral cavities of graeserite. Symbols: large circle represents Ba, medium circle is As, and small circles are O sites. The O(5) site is highlighted and it is shown as light blue circles. For the sake of completeness, labels of the other O sites forming the cavities are shown in (a).